On the theoretical basis of perfusion measurements by dynamic susceptibility contrast MRI

1 AUTHOR:

Valerij Kiselev

Universitätsklinikum Freiburg

76 PUBLICATIONS **1,656** CITATIONS

SEE PROFILE

On the Theoretical Basis of Perfusion Measurements by Dynamic Susceptibility Contrast MRI

V.G. Kiselev*

A quantitative analysis was undertaken to calibrate the perfusion quantification technique based on tracking the first pass of a bolus of a blood pool contrast agent. A complete simulation of the bolus passage, of the associated changes in the T_2 and T_2^* signals, and of the data processing was performed using the tracer dilution theory, an analytical theory of the MR signal from living tissues and numerical simulations. The noise was excluded in the simulation in order to analyze the ultimate accuracy of the method. It is demonstrated that the relationship between the contrast agent concentration and the associated changes in the transverse relaxation rate shows essentially different forms in studied tissue and in the reference artery. This effect results in systematic deviations of the measured blood flow, blood volume, and the residue function obtained with conventional processing from their true values. The error depends on the microvascular composition, the properties of the contrast agent, and the weights of the various compartments in the total signal. The results show that dynamic susceptibility contrast MRI can reach the goal of absolute perfusion quantification only with additional input from measurements of the microvascular architecture. Alternatively, the method can be used to provide such information if the perfusion is quantified by another modality. Magn Reson Med 46: 1113–1122, 2001. © 2001 Wiley-Liss, Inc.

Key words: perfusion imaging; dynamic MRI; bolus tracking; T_2 contrast; susceptibility contrast

Magnetic resonance imaging (MRI) of the first passage of a bolus of a blood pool contrast agent is a promising method for assessment of regional perfusion (1,2). This method implies a measurement of the contrast agent concentration time course in both a volume of interest (VOI) and a feeding artery. The quantification of the perfusion is achieved by comparison of these data sets. The underlying theory rests on two basic assumptions. First, it is assumed that the measured MR signal is proportional to the concentration of the contrast agent, with a universal proportionality coefficient for both the VOI and a reference voxel in the artery. Second, the kinetic of the contrast agent is described in terms of a linear model. The aim of this work is to demonstrate that the former assumption is invalid in proton MRI: the relationship between the MRI signal and the concentration of the contrast agent in the VOI significantly differs from that in the reference voxel. It depends on the MRI pulse sequence and the vascular composition of the investigated tissue.

The reason for such variability in the MRI signal is the contribution of the extravascular protons. These parenchymal protons are dephased by the blood pool contrast agent through the inhomogeneous, long-ranged, susceptibility-induced magnetic field. Thus, their contribution to the MR signal follows the time course of the contrast agent concentration with a specific functional dependence that significantly differs from the relaxation effect of the contrast agent in blood. This peculiarity is not accounted for in the present theory (1,3).

Until now, theoretical interest has been focused on the so-called deconvolution procedure in the presence of noise. This issue is well understood (3) and is not considered here. The presented results were obtained for a noise-free simulation. This allows analysis of the inherent accuracy of the method. The obtained theoretical predictions are compared with published experimental data (4–6).

METHODS

Tracer Dilution Theory

Let us start with a brief review of the tracer dilution theory (7). Consider a VOI and a voxel inside a properly chosen supplying artery. Let us denote as $c_a(t)$ and $c(t)$ the concentrations of the contrast agent in the artery and in blood in the studied tissue, respectively. The concentration $c(t)$ linearly depends on the history of $c_a(t)$. This is expressed as a convolution with a kernel $h(t)$ which describes the blood transport:

$$c(t) = \int_{-\infty}^{t} h(t - \tau)c_a(\tau)d\tau. \qquad [1]$$

In practical calculations the lower limit in this integral can be replaced with the moment of bolus injection. The function $h(t)$ possesses a property

$$\int_{0}^{\infty} h(t)dt = 1 \qquad [2]$$

which reflects the fact that $c = c_a$ if both concentrations are constant in time. Integration of Eq. [1] over t with account for this property leads to a useful relation

$$\int_{-\infty}^{\infty} c(t) = \int_{-\infty}^{\infty} c_a(t). \qquad [3]$$

This equation results in a widely used formula for the calculation of the blood volume fraction ζ. Suppose that the average concentration of the contrast agent in the VOI, denoted hereafter as $\bar{c}(t) = \zeta c(t)$, is known. Then

Section of Medical Physics, Department of Diagnostic Radiology, University Hospital Freiburg, Freiburg, Germany.
*Correspondence to: Dr. V.G. Kiselev, Section of Medical Physics, Department of Diagnostic Radiology, University Hospital Freiburg, Hugstetterstr. 55, D-79106 Freiburg, Germany. E-mail: kiselev@ukl.uni-freiburg.de

$$\zeta = \frac{\int_{-\infty}^{\infty} \bar{c}(t)}{\int_{-\infty}^{\infty} c_a(t)}. \qquad [4]$$

The average concentration $\bar{c}(t)$ can be expressed in terms of $h(t)$ by applying Eq. [1] to the draining veins of the VOI and calculating the amount of contrast agent in the pool between these veins and the feeding reference artery:

$$\bar{c}(t) = f \int_{-\infty}^{t} \mathcal{R}(t - \tau) c_a(\tau) d\tau. \qquad [5]$$

Here f is the blood flow measured in ml/100 ml/min and

$$\mathcal{R}(t) = 1 - \int_{0}^{t} h(\tau) d\tau \qquad [6]$$

is a kernel called the residue function. It is equal to the fraction of the inflowed contrast agent, which remains in the VOI after the time $t.$ By this meaning it should monotonously decrease from $\mathcal{R}(0) = 1$ to $\mathcal{R}(\infty) = 0$. The latter property states the complete washout of the contrast agent in a sufficiently long time. The integral $\int \mathcal{R}(t) \, dt$ is equal to the mean transit time T of blood from the arterial to the venous pool. Integration of Eq. [5] with an account for Eq. [3] results in the central volume principle $\zeta = fT$.

In the MR technique the concentrations $c_a(t)$ and $\bar{c}(t)$ are measured by the associated increases in the transverse relaxation rates in the artery R_{2a} and the VOI R_2. The central assumption of the dynamic perfusion measurements is a universal linear dependence between the relaxation and the concentration for both the reference voxel and the VOI:

$$R_{2a}(t) = rc_a(t) \text{ and } R_2(t) = r\bar{c}(t). \qquad [7]$$

The proportionality coefficient r is the relaxivity. By virtue of this assumption, the concentrations in Eqs. [4] and [5] are replaced with the measured changes in the corresponding MR signals according to the formula

$$\bar{c}(t) = -\frac{1}{rT_E} \ln \frac{s(t)}{s(0)} \qquad [8]$$

and an analogous one for $c_a(t)$. Here T_E is the echo time, $s(t)$ is the measured MR signal time course, and $s(0)$ is the baseline value before the bolus passage. As explained in the Introduction, the assumption of equal relaxivity in the reference artery and the VOI is incorrect. Let us label all values obtained by means of Eq. [8] with a subscript "app" (an abbreviation for "apparent") to contrast the true values written without subscript. These are ζ_{app}, f_{app}, $\mathcal{R}_{app}(t)$, $\bar{c}_{app}(t)$, and ζ, f, $\mathcal{R}(t)$, $\bar{c}(t)$, respectively. The aim of this study can now be reformulated as to find the relationship between the apparent values and their true counterparts.

Tissue Model

The tissue is modeled with three main compartments: blood in vessels, parenchyma, and a nonperfused compartment, which does not change its properties during the bolus passage. The latter models the CSF in the brain. The blood and parenchyma occupy a partial volume p of the VOI. Within this combined compartment the blood occupies a volume fraction ζ. The vascular network consists of three pools: arteries, capillaries, and veins, with the volume fractions ζ_a, ζ_c, and ζ_v, respectively. This microvascular composition needs to be further specified because the MR signal depends on the vessel radius. Let us introduce the differential volume fractions $\zeta_a(\rho)$, $\zeta_c(\rho)$, and $\zeta_v(\rho)$ of vessels with radius ρ. These functions obey a normalization condition

$$\int_{0}^{\infty} \zeta_\alpha(\rho) d\rho = \zeta_\alpha \qquad [9]$$

where α labels the three blood pools: $\alpha = a$, c, v. The calculation of the MR signal from each compartment is described below. Further input parameters are the true blood flow f and the residue function $\mathcal{R}(t)$.

Outline of Simulation

The starting point of the analysis is the time course of the contract agent concentration in the artery $c_a(t)$. It provides an increase in the relaxation rate in blood according to the first equality in Eq. [7]. It is assumed that the relaxivity r is known from in vitro measurements.

The concentration $c(t)$ in blood is calculated as $c(t) = \bar{c}(t)/\zeta$, using Eq. [5] for $\bar{c}(t)$. This defines both the relaxation in blood, which is the same as in Eq. [7], and the magnetic susceptibility of blood χ as

$$\chi = \chi_0 + kc(t). \qquad [10]$$

Here χ_0 is the natural susceptibility of blood, which equals zero in the arterial pool and is nonzero in veins. The coefficient k is supposed to be measured in vitro.

The first round of analysis is not sensitive to the details of the dependence of the MR signal on χ. The only used theoretical result is the additiveness of the microvasculature contribution to the relaxation rate in the parenchyma, which takes the form $R_{2p0} + R_{2p}$ (8–10). The quantity R_{2p0} is the rate of relaxation caused by the spin-spin interactions at the molecular scale. This rate can be measured with the Carr-Purcell-Meiboom-Gill sequence (11) with a vanishing interecho interval. In turn, the susceptibility effect of vessels R_{2p} is a sum of contributions of each of the three blood pools:

$$R_{2p} = R_{2pa} + R_{2pc} + R_{2pv} \equiv \sum_\alpha R_{2p\alpha}. \qquad [11]$$

The above formulae are written for the true relaxation rates measurable in the spin-echo (SE) experiments. Analogous formulae for the gradient-echo (GE) measurements have the same form, with a star symbol added. To avoid

duplications, such formulae are omitted throughout this work. The equations below are applicable to both the SE and the GE sequences unless otherwise stated.

The total MR signal from the VOI takes the form

$$s(t) = p\{(1 - \zeta)\exp[-(R_{2p0} + R_{2p})T_E] + \zeta \exp(-R_{2b}T_E)\}$$
$$+ (1 - p)\exp(-R_{2w}T_E) \quad [12]$$

where R_{2b} is the total relaxation rate in blood, and R_{2w} the relaxation rate in the nonperfused compartment. This formula leads to a general analytical dependence between f_{app} and f, as presented in the Results section. This dependence is specified at the next step using the theoretical model (8–10) for the relaxation rates.

Up to this point the theoretical analysis is duplicated by numerical simulations. The further computations are numerical. The obtained $c(t)$ is used to calculate the MR signal using Eq. [12] and an extension of the analytical formulae (8–10) for R_{2p}, as described below. Then the conventional processing (1) of this simulated signal yields the apparent values $\mathcal{R}_{app}(t)$, f_{app}, and ζ_{app}.

Calculation of the Intravascular Signal

The intravascular signal is a sum of three monoexponential contributions from the arterial, capillary, and venous pools weighted with their volume fractions. Thus, the rate R_{2b} in Eq. [12] is only a place-hold notation. The relaxation rate in the arterial pool is described by the first equality in Eq. [7], which is the same as for the arterial reference voxel. Explicitly, $R_{2a} = R_{2a0} + rc(t)$, where the first term describes the relaxation in arterial blood without the contrast agent. The relaxation rate in the venous blood takes a similar form $R_{2v} = R_{2v0} + rc(t)$. Both R_{2a0} and R_{2v0} are taken from in vitro measurements (12).

The signal from the capillary pool s_c is calculated by a linear interpolation of the relaxation rate between the arterial and venous ends. This gives

$$s_c = \zeta_c \frac{\exp(-R_{2a0}T_E) - \exp(-R_{2v0}T_E)}{(R_{2v0} - R_{2a0})T_E} \exp[-rc(t)T_E].$$
$$[13]$$

The bulk susceptibility of venous blood results in oscillations of the blood signal measured with the GE technique. This can be described with an additional factor (10). It takes the form

$$\left(\frac{\pi}{4\omega T_E}\right)^{1/2} \cos\left(\frac{\omega T_E}{3} - \frac{\pi}{4}\right) \quad [14]$$

for $\omega T_E \gg 1$ and can be continued to $\omega T_E = 0$ to interpolate the numberical result of Ref. 10. The blood frequency offset is neglected in the major part of the present simulation for the following reasons. The oscillation period obtained from Eq. [14] is close to 200 ms for $B_0 = 1$ T and the values given below in the Numerical Values of Parameters section. As it is larger than the typically used T_E, the oscillations effectively modify the signal relaxation. During the bolus passage, the blood magnetic susceptibility

increases by more than an order of magnitude, and the period becomes shorter than the T_E. In this case the frequency offset results in an apparent displacement of the blood vessels—for example, one in the phase-encoding direction in the EPI technique. An appropriate modification of the point spread function is beyond the scope of this work.

Further uncertainty comes from the fact that the capillaries cannot be described with the bulk blood parameters implied in Eq. [14]. An analytic approach developed in Ref. 9 suggests that the frequency offset in the capillary network is suppressed relative to its relaxation effect by a factor of ωt_D for $\omega t_D \ll 1$. More detailed predictions are not currently available. The blood frequency offset as described by Eq. [14] is included only for an assessment of its effect. To this end Eq. [14] is applied to the arterial and venous pools, while the capillary contribution remains unchanged.

Calculation of the Extravascular Signal

The extravascular signal is calculated by means of an analytical theory of the MR signal developed in Refs. 8–10. According to this theory, the effect of microvessels on the parenchymal relaxation rate is additive and takes the following form:

$$R_{2p\alpha} = \int d\rho \, \zeta_\alpha(\rho) r_{2\alpha} \quad [15]$$

for each of the three blood pools in Eq. [11]. The functions $r_{2\alpha}$ are the relaxivities of vessels of a given type and radius ρ defined as the relaxation rate per unit volume fraction. These functions may depend on T_E. The combination $T_E r_{2\alpha}$ in Eq. [15] is defined by the dephasing effect of a single vessel. Each vessel is characterized by two parameters: the time of diffusion across the vessel $t_D = \rho^2/D$, and the characteristic shift of the Larmor frequency on the surface of the vessel $\omega = 2\pi\chi\gamma B_0$. The relaxation effect of the vessel depends on these values and T_E via two dimensionless combinations: T_E/t_D and ωt_D. The latter gives the order of magnitude of the phase acquired by a diffusing proton after passing the vessel. The theory provides analytical results in two extreme cases called the diffusional narrowing regime (DNR) and the static dephasing regime (SDR) (Fig. 1). Let us consider them in more detail.

The SDR implies that the proton diffusion length $l_D = (DT_E)^{1/2}$ is much shorter than the vessel radius. Then the dephasing of a spin packet occurs in a uniform gradient of the magnetic field. The vessel relaxivity for the free induction decay (FID) reads (8)

$$T_E r_{2\alpha}^* = \frac{2}{15} (\omega T_E)^2 \quad [16]$$

for $\omega T_E \ll 1$ and

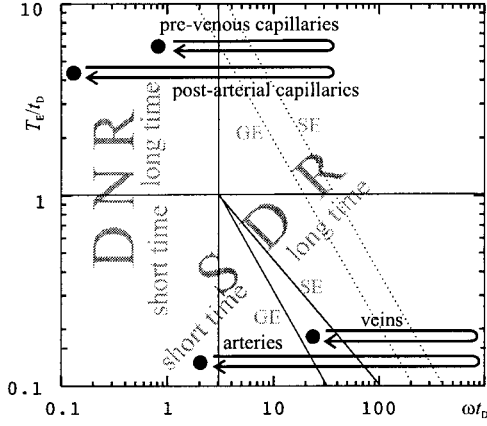$$T_E r_{2\alpha}^* = \frac{2}{3} \omega T_E - 1 \quad [17]$$

FIG. 1. A schematic representation of the dephasing regimes for tissues with low blood volume fraction. The relaxivity, which is defined as the relaxation per unit vessel volume fraction, depends on two parameters: ωt_D and T_E/t_D. Two quadrants below the horizontal line $T_E/t_D = 1$ correspond to the SDR, in which the diffusion length is shorter than the vessel radius. The upper right quadrant shows the extension of the applicability range of the SDR to $\omega t_D \gg 1$, as discussed in the Calculation of the Extravascular Signal section and in the caption for Fig. 2. The vertical line separates the SDR from the DNR, which is valid for $\omega t_D \ll 1$. The boundary is positioned at $\omega t_D \approx 3$, accounting for the results of the Monte Carlo simulation (13) partially reproduced in Fig. 3. For simplicity, the finite crossover thicknesses are not shown. The SDR and DNR overlap in the lower left quadrant. The solid biased lines represent the transitions between the short-time (Eqs. [16] and [17]) and the long-time (Eqs. [18] and [19]) asymptotic forms of the SDR. The analogous boundary for the DNR is just $T_E/t_D \approx 1$. The dotted lines represent the mapping of the parameter range probed by the results of Monte Carlo simulation (13) (Fig. 3). The actual length of these lines spans about one decade above and below the figure frame. The thick lines with arrows represent the evolution of the three vessel groups during the bolus passage. The initial and final states are indicated by filled circles. The ascending and descending branches are separated for clarity.

comes from the spins for which $\phi \sim 1$. These are located at the distances $\rho \sim (\omega T_E)^{1/2}\rho_0$. A comparison of the diffusion length with ρ gives $l_D/\rho \sim (\omega t_D)^{-1/2} \ll 1$. This validates the approximation of the static dephasing. For the SE the dephasing is determined by the variation of the Larmor frequency over the diffusion length such that $\phi \sim \omega T_E\rho_0^2 l_D/\rho^3$. A comparison of l_D with the distance ρ, at which $\phi \sim 1$, yields $l_D/\rho \sim (\omega t_D)^{-1/3} \ll 1$. To sum up, the SDR is always valid for short T_Es. If the MR signal reaches its long-time asymptotic form (Eqs. [17] and [19]) within this regime, it remains valid for arbitrary long T_E.

The DNR takes place for the weak dephasing $\omega t_D \ll 1$. The vessel relaxivity reads (9)

$$T_E r_{2\alpha}^* = \frac{4}{45}(\omega t_D)^2\left[\frac{T_E}{t_D}\left(\ln\frac{T_E}{t_D} + 0.309\right) + \frac{1}{4}\ln\frac{T_E}{t_D} + 0.619\right]$$

[20]

for the FID and

$$T_E r_{2\alpha} = \frac{8}{45}(\omega t_D)^2\left[\frac{T_E}{2t_D}\left(\ln\frac{T_E}{2t_D} - 0.384\right) + \frac{1}{4}\ln\frac{T_E}{2t_D} + 0.619\right]$$

[21]

for the SE relaxation. As follows from a comparison of this theory with the results of a Monte Carlo simulation (13), the crossover between the DNR and the SDR occurs in the range $\omega t_D \approx 6$ (Fig. 3).

Let us list the dephasing regimes for each vessel group during the bolus passage (Fig. 1). For the capillaries the DNR is applicable at low $c(t)$. The postarterial capillaries are deeper in this regime due to their very low natural magnetic susceptibility. The increase in $c(t)$ during the bolus passage transfers the relaxation to the SDR. An interpolation formula (Eq. [35]), which is given in the Ap-

for $\omega T_E \gg 1$. In the SE measurement the relaxivity takes the form (10)

$$T_E r_{2\alpha} = \frac{1}{15}(\omega t_D)^2\left(\frac{T_E}{t_D}\right)^3$$

[18]

for $(\omega t_D)^{2/3} T_E/t_D \ll 1$ and

$$T_E r_{2\alpha} = 0.694(\omega t_D)^{2/3}\frac{T_E}{t_D} - 1$$

[19]

for $(\omega t_D)^{2/3} T_E/t_D \gg 1$.

In terms of the T_E, the above-written condition for the static dephasing reads $t_D/T_E \gg 1$. This range can be extended up to $\omega t_D \gg 1$, as illustrated in Figs. 1 and 2. Consider the attenuation of the MR signal from the protons affected by a single vessel of the radius ρ_0 to the time moment $T_E \gg 1/\omega$ (Fig. 2). For the FID the characteristic phase difference ϕ induced by the presence of the vessel is on the order of $\omega T_E\rho_0^2/\rho^2$ at the distance ρ from the vessel. The protons near the vessel have $\phi \gg 1$ and are completely dephased. The main contribution to the relaxation rate
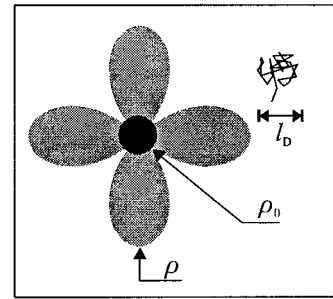

FIG. 2. Extension of the applicability range of the SDR from the short diffusion lengths $l_D \ll \rho_0$ to $\omega T_E \gg 1$. A cross-section of a vessel of radius ρ_0 is shown with the black circle. The folded line represents a packet of diffusing spins. The span of the diffusion motion is $l_D = (DT_E)^{1/2}$. The spins within the gray region are effectively dephased, while the spins outside this region contribute to the signal. The signal attenuation can be considered as a growth of the dephased area. Thus, the relaxation rate is dominated by its boundary and the diffusion length should be compared with its size, which is $\rho \gg \rho_0$. The static dephasing takes place when $l_D \ll \rho$ rather than $l_D \ll \rho_0$, which is the case illustrated in the figure. This condition is equivalent to $\omega T_E \gg 1$, as explained in the Calculation of the Extravascular Signal section.
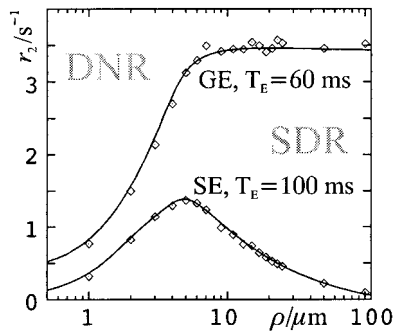
FIG. 3. Relaxation rate in a simulated tissue as a function of the radius ρ of monosized vessels for the GE and SE measurements. The points show the results of the Monte Carlo simulation (13). The lines were obtained using the interpolation formulae in Eq. [35] for the dephasing of the extravascular protons. These formulae are used here for the calculation of the relaxation effect of capillaries (crf. Fig. 1). A deviation from the Monte Carlo point at $\rho = 100$ μm for the SE is due to poor applicability of the long time asymptotic form (Eq. [19]) (crf. Fig. 1). This imperfection does not affect the presented calculations because no capillaries, for which Eq. [35] is used, gets in this dephasing regime, as seen in Fig. 1. The parameters are $B_0 = 1.5$ T, $\zeta = 2\%$, $\chi = 10^{-7}$, $D = 1$ μm²/ms, $T_E = 60$ ms for the GE, and $T_E = 100$ ms for the SE. The walls of the vessels are impermeable.

pendix, is used to bridge over the transition region (Fig. 3). The trajectories of veins and arteries in Fig. 1 move right-downwards from that of capillaries according to the increased diameter. Thus, the major part of these vessels falls into the SDR. For both the veins and arteries interpolation formulae (Eqs. [31] and [32]) are applied to describe the transition between the short (Eqs. [16] and [18]) and long (Eqs. [17] and [19]) asymptotic forms, as illustrated in Fig. 4.

Numerical Values of Parameters

Unless otherwise stated, the following parameters are used in the numerical calculations. The main magnetic field $B_0 = 1$ T, and $T_E = 45$ ms for the GE and 75 ms for the SE measurements were chosen to match the calibration experiments (4–6).

The blood flow was set to $f = 80$ ml/100 g/min. The minor difference between the units of ml/100 g/min and ml/100 ml/min is neglected throughout this paper. The partial volume of the parenchyma was assigned a value of $p = 0.9$, and the diffusion coefficient $D = 0.8$ μm²/ms (14).

A proper simulation of the microvasculature requires a knowledge of the detailed vessel size distribution as it follows from Eq. [15]. It is available for capillaries in animal models (16). For the present study a monosized distribution was chosen with the radius $\rho_c = 3.5$ μm at 2% volume fraction ($\zeta_c = 0.02$), which is close to the typically reported average values for the human brain. Unfortunately, the author has not found any directly acquired differential volumetric data for the whole arterial and venous systems. In order to construct a model for the vessel size distribution, recent information (17) concerning the self-similarity structure of the vascular system was used. Following the assumptions of Ref. 17, the whole arterial

and venous trees possess scaling relations that result in equal volume fractions of vessels of all sizes. This implies that both $\zeta_a(\rho_a)$ and $\zeta_v(\rho_v)$ are constant. An estimate of these values can be obtained with a formula derived in Ref. 17 that relates the vein caliber to the cortical area A it drains: $2\rho_v = [(A/\text{mm}^2)^{1/3}/8]$mm. Applying this formula to an area of 600 mm², which represents a region of interest in the brain rather than in a voxel, results in $2\rho_v = 1$ mm. The vessels on the order of, or larger than this size cannot be considered within the statistical approach of the present study, and thus provide an upper limit on the vessel size accounted for in the model. On the other hand, the above formula gives $2\rho_v = 5$ mm for a significant part, such as one-quarter of the total cortical area, which is equal to 2430 cm² (15). Thus, the portion of the venous and arterial vascular volume, which is accounted for by the present model, is about one-fifth of the total one. The latter is 6–8%, with 80–93% in the venous and arterial pools (18,19). Therefore, the resulting estimate is $\zeta_a + \zeta_v \approx 0.01$.

Another estimate of this value can be obtained from the results of a recent study (20), in which an average vessel size in the rat brain was deduced by comparison of R_2 and R_2^*. The reported value, called the vessel size index, is R = 4.77 μm. This is larger than the expected pure capillary index $R_c = 3.31$ μm (20) by the contribution of larger vessels. To make use of this difference, note that Eq. [19] holds for all vessels at high concentrations of the contrast agent used in Ref. 20. Thus the vessel size index reflects the averaging of the vessel radii to the power $-2/3$: $R^{-2/3} =$
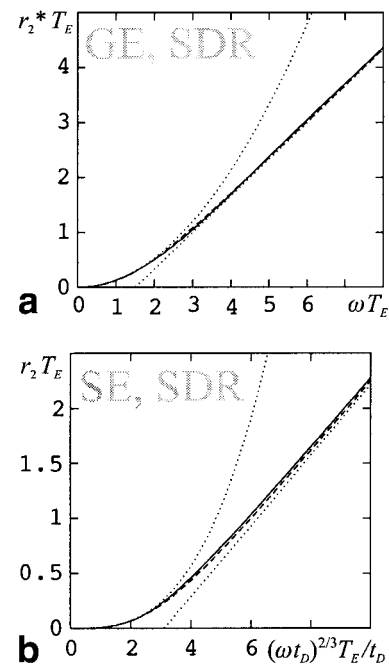

FIG. 4. The relaxation exponent $r_2^* T_E$ in the static dephasing regime for (**a**) the FID and $r_2 T_E$ for (**b**) the SE measurement. The solid lines represent the theoretical results found with a numerical integration (10). The dashed lines show the interpolation formulae (Eqs. [31] and [32]) that are used here to calculate the signal from arteries and veins (crf. Fig. 1). The asymptotic formulae (**a**) Eqs. [16] and [17] and (**b**) Eqs. [18] and [19] are shown with the dotted lines.

$\langle \rho^{-2/3} \rangle$. This gives R $\approx$ R$_c$(1 + x)$^{3/2}$, where $x = (\zeta_a + \zeta_v)/\zeta_c$. Finally, $x \approx 0.2$ leads to a very small noncapillary volume fraction of 0.4%. This is a rather rough estimate because the capillary radius distribution used in Ref. 20 was taken from another study (21). However, it practically rules out the volume fraction of veins and arteries in a parenchymal voxel that exceeds ζ_c. With an account for the presented estimates and for the conventionally-used model parameters (13,22), the volume fractions of the venous and arterial pools were set to $\zeta_v = 0.01$ and $\zeta_a = 0.005$.

The continuous vessel radius distributions can be replaced by monosized distributions with a representative radius. This value is not significant for the GE technique because R_2^* does not depend on the size of the large vessels (Eq. [17]). For the SE experiment, the vessel size index of separated arterial or venous pools should be used. It is close to the maximal radius, which is about 500 μm, as discussed above, divided by $3^{3/2} \approx 5$. This results in $\rho_v = \rho_a = 100$ μm assumed in the present model.

The magnetic susceptibility of venous blood was assigned according to a recent result (12) for the conditions close to that met in vivo: $\chi_0 = 0.038$ ppm. This value is the product of the reported susceptibility of the fully deoxygenated blood, which equals 0.108 ppm, and the 35% oxygen extraction, which enters the formulae as the difference in the oxygenation levels between arteries and veins. (All magnetic values are measured in the CGS units. To convert them to SI units the given numbers should be multiplied by 4π). To simulate the change of the magnetic susceptibility in the capillary pool, the venous value of χ was assigned to one-half of the capillary volume, and the arterial χ to the other half.

The simplest exponential form was chosen for the residue function:

$$\mathcal{R} = \exp(-t/T). \qquad [22]$$

The mean transit time T is defined by the central volume principle $T = \zeta/f \approx 2.6$ s.

The microscopic contribution to the relaxation rate in parenchyma and arterial blood R_{2p0} was chosen to be 16.7 s^{-1} (= 1/60 ms) for the GE 10 s^{-1} for the SE at 1.5 T, and rescaled down to 1 T proportionally to B_0^2. This gives 11.1 s^{-1} and 6.7 s^{-1}, respectively. The baseline relaxation rates in the arteries R_{2a0} and the veins R_{2v0} were calculated from the empiric formula $R_{2v0} = (6.2 + 59\, E_0^2)$ s^{-1} (12), in which E_0 is the oxygen extraction fraction. The values measured at $B_0 = 1.5$ T were downscaled proportionally to B_0^2. This resulted in $R_{2a0} = 2.76$ s^{-1} and $R_{2v0} = 5.97$ s^{-1}. For blood the validity of such a conversion follows from many reports (23,24), and from the quadratic dependence of the relaxation rate on the blood oxygenation level observed in Ref. 12. The dependence of R_{2p0} on B_0 is less clear, as R_{2p0} is only one of many contributions to the measurable relaxation rate. Theoretical reasons (25) suggest a range of possibilities from constant to quadratic dependence. A linear relationship has been found in postmortem blood-free monkey brain specimens (24) and is assumed in the present study, although the limitations of such a transfer are understood. The difference between the GE and SE relaxation rates in blood is neglected.

Gd-DTPA has been considered as the contrast agent. The relaxivity and volume susceptibility of this substance have been measured in a number of experiments. In this study, the results obtained by van Osch et al. (26) in an in vitro GE experiment were used. The values are $k = 0.024$ ppm/mM and $r = 2.7$ s^{-1} μM^{-1}. The latter was rescaled proportionally to B_0^2 from the reported value $r = 6.0$ s^{-1} μM^{-1} at 1.5 T. The fine nonlinearity of the relaxation effect (26,27) is neglected here.

The input bolus was given the form

$$c_a(t) = c_{\max} t \exp(-t/t_0 + 1) \qquad [23]$$

where the time constant $t_0 = 7$ ms. The peak concentration was set to $c_{\max} = 18$ mM, which most probably corresponds to the dose 0.2 mmol/kg of 500 mM solution injected within 1 s (28).

The numerical convolution and deconvolution were performed by fast Fourier transformation. A rather fine grid on the time and frequency axes was used to approach the continuous integrals with three significant digits. In most of the simulations a time interval of 200 s was represented with 2056 points.

RESULTS

Apparent Blood Flow and Residue Function

Let us consider those general properties of $\mathcal{R}_{\mathrm{app}}(t)$ which follow from the mathematical nature of the deconvolution. The first aim is to show that the blood flow is defined by the linear response of the MR signal to small changes in the concentration of the contrast agent. To this end, note that Eq. [5] forms a triangular system of linear equations for the unknown function $f\mathcal{R}_{\mathrm{app}}$ provided $c_a(t)$ is measured and $\bar{c}(t)$ is replaced with the known values of $\bar{c}_{\mathrm{app}}(t)$. This becomes obvious in the discrete version of Eq. [5]. Let time after the beginning of the bolus passage be incremented as $t = \Delta t, 2\Delta t \ldots$. Then Eq. [5] takes the form

$$\bar{c}_{\mathrm{app}}(\Delta t) = f\mathcal{R}_{\mathrm{app}}(0)c_a(\Delta t)\Delta t \qquad [24]$$

$$\bar{c}_{\mathrm{app}}(2\Delta t) = [f\mathcal{R}_{\mathrm{app}}(0)c_a(2\Delta t) + f\mathcal{R}_{\mathrm{app}}(\Delta t)c_a(\Delta t)]\Delta t \qquad [25]$$

and so on. The initial value $f\mathcal{R}_{\mathrm{app}}(0)$ is defined from Eq. [24], and then $f\mathcal{R}_{\mathrm{app}}(\Delta t)$ is found from Eq. [25], etc. The blood flow is defined by using the normalization condition $\mathcal{R}_{\mathrm{app}}(0) = 1$. It is therefore determined by the initial small increases in $c_a(t)$ and $\bar{c}_{\mathrm{app}}(t)$.

This allows a general relationship to be found between f_{app} and f by a substitution of Eq. [12] into Eq. [8]. An expansion in $c(t)$ gives a linear relation

$$\bar{c}_{\mathrm{app}}(t) = \mathrm{Coeff} \cdot c(t) \qquad [26]$$

in which the coefficient takes the form

$$\mathrm{Coeff} = \left[w_b + w_p \frac{k}{r} \sum_\alpha \int d\rho \zeta_\alpha(\rho) \frac{dr_{2\alpha}}{d\chi} \right]. \qquad [27]$$

Here

$$w_b = \frac{p\zeta\,\exp(-R_{2b}T_E)}{s(0)} \text{ and } w_p = \frac{p\cdot(1-\zeta)\exp(-R_{2p}T_E)}{s(0)}$$

$$[28]$$

are the weights of the blood and parenchyma in the signal (Eq. [12]) measured before the bolus passage, k is defined in Eq. [10], and the derivatives are taken at $c = 0$. Comparison of Eqs. [26] and [5] yields finally

$$f_{app} = \frac{\text{Coeff}}{\zeta}\,f.$$

$$[29]$$

Further development of this formula requires knowledge of the derivatives $dr_{2\alpha}/d\chi$ in Eq. [27]. The contribution of the arterial pool to the relaxation rate R_{2pa} is proportional to χ^2 according to Eqs. [16] and [18]. The point $c(t) = 0$ corresponds to $\chi = 0$ because of the diamagnetism of arterial blood ($\chi_0 = 0$). Thus, the arterial contribution in Eq. [29] vanishes. This is not the case for the capillary and venous pools, in which $\chi_0 \neq 0$. A power law dependence $r_{2\alpha} \propto \chi^{\nu_\alpha}$ results in $dr_{2\alpha}/d\chi = \nu_\alpha r_{2\alpha}/\chi_0$. Consequently, f_{app} (Eq. [29]) takes the form

$$f_{app} = \frac{1}{\zeta}\left[w_b + w_p\,\frac{k}{r\chi_0}\,(\nu_v R_{2pv} + \nu_c R_{2pc}) \right] f.$$

$$[30]$$

The values of ν_c and ν_v depend on the measurement type and parameters. For the typical measurements at B_0 below 2 T the theory predicts $\nu_c = 2$ (Eqs. [20] and [21]). The vein contribution is more variable. For low fields $\nu_v = 2$ (Eq. [16]) due to small ω. For high fields $\nu_v = 1$ (Eq. [17]) and $\nu_v = 2/3$ (Eq. [19]) for the GE and SE, respectively.

An evaluation of Eq. [30] for the GE measurement with $\nu_v = \nu_c = 2$ results in $f_{app} = 4.98f$, while the numerical simulation gives $f_{app} = 4.61f$. The 8% difference is attributed to the too-high values of ν, which are in reality below 2. The found coefficient consists of two main contributions according to the way the contrast agent affects the MR relaxation rate. The variation of the relaxation rate in blood gives 25%. The remaining 75% is due to the change in the parenchymal signal by the susceptibility-induced magnetic fields during the bolus passage. This contribution is shared by the capillaries (29%) and veins (46%). The arteries give 0.2%, which is within the computation error. Numerical simulation confirms the independence of f_{app} on the forms of $c_a(t)$ and $\mathcal{R}(t)$.

The analogous results for the SE measurement are as follows. An evaluation of Eq. [30] with $\nu_v = \nu_c = 2$ results in $f_{app} = 1.75f$, while the numerical simulation gives $f_{app} = 1.71f$. The blood and parenchymal contributions in the coefficient 1.71 are 59% and 41%, respectively. The capillaries, veins, and arteries give 40%, 1%, and 0.003%, respectively.

Accounting for the frequency offset in the blood pool results in a modification of the intravascular contribution on the right side of Eqs. [27] and [30] for GE sequences. Numerically, the apparent blood flow increases from $4.61f$ to $f_{app} = 5.50f$.

As follows from Eqs. [16], [18], and [19], the MR signal is a nonlinear function of $c(t)$. This affects the shape of

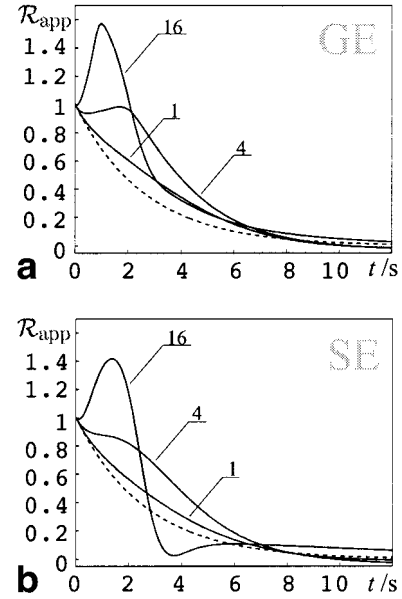**FIG. 5.** The apparent residue function $\mathcal{R}_{app}(t)$ as a function of time t for various maximal contrast agent concentrations (Eq. [23]) (solid lines labeled with the values of c_{max} in mM) for the (**a**) GE and (**b**) SE measurements. The dashed lines show the actually used residue function $\mathcal{R}(t)$. The odd behavior of $\mathcal{R}_{app}(t)$ for high concentrations is due to the effect of nonlinearity of the MR signal, as discussed in the Apparent Blood Flow and Residue Function section.

$\mathcal{R}_{app}(t)$ (Fig. 5). The apparent contrast agent concentration takes the form $\bar{c}_{app} \approx \text{Coeff} \cdot c(t) + \text{Coeff}_2 \cdot c(t)^2$ for initial times. The first coefficient is defined in Eq. [27]. Assume, for example, that $\mathcal{R} = 1$ and $c_a(t) \propto t$ for small t. As follows from Eq. [5] for this case, $c(t) \propto t^2$ and the nonlinear term in $\bar{c}_{app}$ is proportional to t^4. This results in a term $\mathcal{R}_{app}$ which is proportional to t^2. By the linearity of Eq. [5], this term should be added to the constant $\mathcal{R}_{app}$ found in the linear approximation. This produces a deviation from the true function. A test calculation for the simplified case $T = t_0$ has shown that the appropriate analytical formulae accurately describe the difference $\mathcal{R}_{app} - \mathcal{R}$ for $c_{max} \ll 1$ mM.

Apparent Blood Volume

In contrast to the blood flow, the apparent blood volume ζ_{app} is defined by the integrated signal time course according to Eq. [4]. For small peak concentrations of the contrast agent the relationship between $c_{app}(t)$ and $c(t)$ is linear. This yields $\zeta_{app} = \text{Coeff} \cdot \zeta$ with the coefficient defined in Eq. [27]. The behavior for higher concentrations depends on whether $c_{app}(t)$ is overlinear or sublinear in $c(t)$. The former case results in an increasing, and the latter in a decreasing ζ_{app} as a function of c_{max}. With the field strength considered here, both cases take place (Fig. 6).

The apparent blood volume is marginally affected by the blood frequency offset. When included, it changes, for example, the data point $\zeta_{app} = 28.4\%$ for $c_{max} = 18$ mM in Fig. 6a up to $\zeta_{app} = 29.5\%$.

DISCUSSION

The obtained results form a complete simulation of the bolus passage, the associated changes in the T_2 and T_2^*
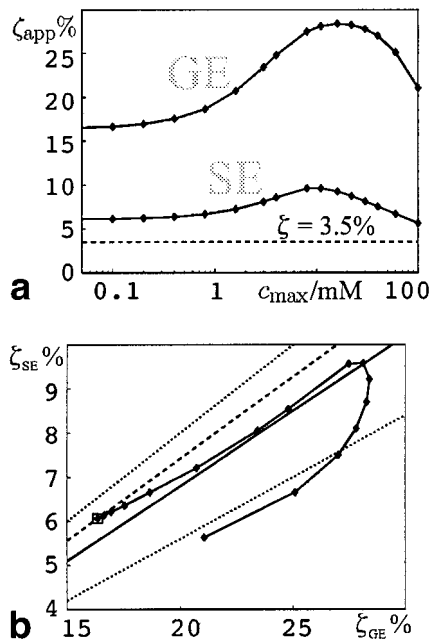
FIG. 6. Dependence of the apparent blood volume on the maximal concentration of the contrast agent c_{max} defined in Eq. [23]. **a:** ζ_{app} as a function of c_{max} for the GE and SE measurements. The dashed line indicates the actually used value of ζ. **b:** A relation between the apparent blood volume measured with the GE and SE techniques as follows from the data shown in **a**. The dependence on c_{max} results from the nonlinearity of the parenchymal relaxation rate in the contrast agent concentration c. A linear relationship would yield a constant ζ_{app}, which is the case for low concentrations (left parts of the curves in **a** and the single box in **b**). The increase in ζ_{app} for the moderate c_{max} is due to the initially quadratic dependence in the concentration c (Eqs. [16] and [18]). For large c the relaxation rate is mainly proportional to c (Eq. [17] for the GE) or to $c^{2/3}$ (Eq. [19] for the SE). This explains a stronger relative decrease in ζ_{app} for the SE data which results in the lower part of the curve in **b**. The dashed line in **b** shows the linear regime for the variable true blood volume. The straight solid line represents the linear dependence with a coefficient of 0.34 ± 0.06, which was experimentally found by manipulating the blood flow (6). The dotted lines show the 1 SD corridor of this result.

signals, and the mathematically exact processing of the acquired noise-free data. This approach shows a systematic deviation of the measured blood flow and blood volume from their true values.

As stated in Eqs. [29] and [30], the measured apparent blood flow is indeed proportional to its actual value, but with a coefficient, which depends on the composition of microvasculature, its relaxation effect, the properties of the contrast agent, and the weights of different compartments in the total signal. The measured blood volume is a more complicated nonlinear function of its true value (Fig. 6). The reason for such an inherent drawback of the currently used data processing scheme is the neglect of the changes in the MR signal from the parenchymal protons, as discussed in the Introduction.

Although the considered effects are specific to the T_2 or T_2^* contrast, they are a manifestation of a general problem of the MR flow measurements, which arises from the fact that the concentration of the MR tracers is measured indi-

rectly via its relaxation effect. The measurement results are affected by the tracer compartmentalization as well as by the spreading of its influence outside its nominal compartment, which usually coincides with the blood pool. The T_2, T_2^*, and T_1 contrasts all suffer from this disadvantage. The spreading is mediated by the susceptibility-induced gradients for the transverse, and by the water exchange between compartments for the longitudinal relaxation. A detailed analysis of T_1 contrast bolus tracking can be found in Ref. 29.

The method of dynamic susceptibility contrast perfusion measurement has been validated against the gold standard of the positron emmision tomography by Østergaard et al. (4,5). The SE technique has shown good agreement between the two modalities (4,5), while the GE technique resulted in an approximately threefold overestimate of the absolute blood flow and volume (6). The present theory predicts a 59% overestimate of the blood flow for the SE and an approximately sixfold overestimate for the GE measurement techniques for the used parameters. This can serve as only an approximate validation of the present theory. The sources of uncertainty are as follows: 1) Possible deviation of the contrast agent properties, which affects the parameters k and r. A proper validation would require an in vitro measurement of these values for each new stock used. 2) An unclear effect of the filtering of the noisy data, either explicit or in the form of fitting of a smooth function to the signal time course (3). The constraint of monotonous decrease of the residue function can also affect the deconvolution procedure. The present theory does not impose such a condition on the apparent function, as shown in Fig. 5. 3) Last, but not least, is a possible mismatch between the microvasculature composition in the subjects of the experimental studies and the parameters used here.

The error seems to be smaller for the relative values due to the linearity of the deconvolution. The ratio between the blood flow measured by the SE and GE techniques was found to be 0.40 ± 0.07 (6). The present theory gives a value of 0.37, in good agreement with the experiment. A linear relationship with a coefficient of 0.34 ± 0.06 has been found between the blood volume measured by the SE and GE techniques over a wide interval of the blood flow (6). The present theory results in a ratio of 0.37 for low peak concentrations of the contrast agent and in very close values up to the assumed concentration of 18 mM (Fig. 6b). Even up to $c_{max} = 100$ mM this ratio remains close to the 1 SD corridor of the experimental result (6), as shown in Fig. 6b. Note that the internal variable in this figure is the peak concentration c_{max}, while the blood flow is kept fixed.

A possible experimental validation of the present theory would be to test parameter dependencies that follow from the general result (Eq. [29]) or from the more specific one given by Eq. [30]. Let us consider some of them in more detail.

A dependence on the MRI parameters, such as B_0 and T_E, enters Eq. [30] via the weights of the blood and parenchymal signal w_b and w_p. This dependence is, however, not very pronounced for the used parameters. For example, a change in the T_E of the GE from 20 ms to 75 ms results in about 10% variations in the simulation results:

from f_{app} = 339 ml/100 ml/min and ζ_{app} = 30% to f_{app} = 379 ml/100 ml/min and ζ_{app} = 27%. Another example illustrates the T_E dependence of the blood volume measured at B_0 = 4 T with the GE technique. An increase of the T_E from 10 to 40 ms results in a change from ζ_{app} = 7.9% to ζ_{app} = 6.0%, with a minor decrease in the apparent blood flow. This is only a rough estimate because the quadratic dependence of the relaxation rate on B_0 should become more linear at high fields (23).

The dependence of the results on B_0 is mainly due to the above effect because the quadratic dependence on B_0 in the relaxivity r in Eq. [30] is canceled by the similar dependence of the relaxation effect of veins R_{2pv} and capillaries R_{2pc}. This is true for the moderate fields below approximately 2 T. For higher fields $R^*_{2pv} \propto B_0$ and $R_{2pv} \propto B_0^{2/3}$, which tends to decrease f_{app} as in the example discussed above for B_0 = 4 T. The results for the typical field strength B = 1.5 T of the clinical scanners are qualitatively similar to those obtained for B = 1 T, with some decrease in the apparent perfusion values. For example, f_{app} = 306 ml/100 ml/min and ζ_{app} = 19% for the GE measurement at B_0 = 1.5 T and rescaled relaxation rates, but with other parameters kept at their default values.

Another possible test point would be to probe the dependence of the apparent blood volume on the maximal concentration of the contrast agent (Fig. 6). This value is the most stable against the noise due to its integral character (Eq. [4]). However, the curve segments near the maxima (Fig. 6a) should be avoided. This requires either high or low doses, with the associated limitations to exclusively animal experiments or the noise level, respectively.

The present theory predicts an odd behavior of the apparent residue function $\mathcal{R}_{app}(t)$ (Fig. 5). For verification, the restriction of the monotonous decrease of $\mathcal{R}_{app}(t)$ should be released during the processing of the experimental data. The noise in the data can also perturb the time course of the calculated residue function. Effective noise control appears to be feasible with the presently used deconvolution techniques (1,3).

CONCLUSIONS

The obtained results show that dynamic susceptibility contrast MRI has not yet reached the goal of absolute perfusion quantification. This method is shown to be highly sensitive to details of microvascular architecture and to weights of various vessel groups in the total relaxation rate. This makes perfusion quantification very challenging. The good side of this finding is that the T_2 or T^*_2 signal variations during bolus passage depend on the same physiological and microanatomical parameters that define the relaxation effect of deoxyhemoglobin. The complex parameter dependence of both contrasts suggests that a complete patient-specific quantification of microcirculation can be achieved in a combined measurement that includes both of these MRI modalities.

APPENDIX

Presented here are the interpolation formulae that were used for the calculations of the relaxation exponent $f = r_2 T_E$. There is no special mathematical rationale behind them other than to provide a reasonable interpolation between theoretically known limits with the account for the results of the Monte Carlo simulation (13). The first formula bridges over the crossover between the short (Eqs. [16] and [17]) and the long (Eqs. [18] and [19]) asymptotic forms, and is applied to arteries and veins (Fig. 4). For the FID the function f depends on a single argument, $x = \omega T_E$. An interpolation formula reads:

$$f(x) = \left[\left(\frac{2}{3} x \right)^5 + \frac{2}{3} x^2 + 1 \right]^{1/5} - 1. \qquad [31]$$

The f-function for the SE relaxation depends on $x = (\omega t_D)^{2/3} T_E / t_D$. An interpolation is achieved with the expression (Fig. 4):

$$f(x) = \left[(0.694x)^5 + \frac{1}{3} x^3 + 1 \right]^{1/5} - 1. \qquad [32]$$

The simulation of capillaries requires additional formulae, which were used to generate Fig. 3. They are to interpolate between Eqs. [17] and [20] and Eqs. [19] and [21], and are described here in a constructive way. The function f depends on both the time parameter $\tau = T_E / t_D$ and the dephasing parameter $z = \omega t_D$. The interpolation occurs between the regions $z \ll 1$ and $z \gg 1$ for each value of τ. As a function of z the f function has the structure $f = \text{Const} \cdot z^v$ (Eqs. [17], [19]–[21]) in both regions, if the term -1 in Eqs. [17] and [19] is neglected for a while. The constant for $z \gg 1$ takes the form $C_{sdr} = 2\tau/3$ and $C_{sdr} = 0.694\tau$ for the GE and SE measurements, respectively. For the small $z \ll 1$ the right sides of Eqs. [20] and [21] read $C_{dnr} z^2$. This is transformed to a positively defined value $C_{dnr+} = (C_{dnr}^2 + a^2)^{1/2}$ with an as yet undefined constant a. The f function for the FID is first approached with the form

$$f_0 = \exp \left(\frac{3z'}{2} - \frac{v}{2} + \frac{1}{2} \ln(C_{sdr} C_{dnr+}) \right.$$
$$\left. + \frac{z'}{2v} \ln \frac{C_{sdr}}{C_{dnr+}} + \left(\frac{3}{2} - \frac{1}{2} v \right) z_0 \right). \qquad [33]$$

Here $z' = z - z_0$, $v = [(z - z_0)^2 + a^2]$ and a constant z_0, which is as yet undefined, determine the position of the crossover between the regions of the static and the diffusion dephasing. Equation [17] requires restoration of the term -1 for large z. The following function is unity for large z and turns sufficiently fast to zero for $z \ll 1$:

$$u = \exp \left[z' - v' + \left(1 - \frac{z'}{v'} \right) z_0 \right] \qquad [34]$$

where $v' = [(z - z_0)^2 + 8a^2]^{1/2}$. Finally,

$$f = f_0 - [1 - (1 - u)^2][1 + (1 - u)]u. \quad [35]$$

The parameters a and z_0 in this formula were adjusted to fit the results of the Monte Carlo simulation (13), as shown in Fig. 3. This resulted in $a = 0.8$ and $z_0 = 1.4$.

The SE relaxation is described by the same formula, with the following modification of the function f_0:

$$f_0 = \exp\left(\frac{4z'}{3} - \frac{2v}{3} + \frac{1}{2}\ln(C_{sdr}C_{dnr+}) + \frac{z'}{2v}\right.$$
$$\left.\ln\frac{C_{sdr}}{C_{dnr+}} + \left(\frac{4}{3} - \frac{2}{3}v\right)z_0\right) \quad [36]$$

with the parameters $a = 0.7$ and $z_0 = 1.6$.

REFERENCES

1. Østergaard L, Weisskoff RM, Chesler DA, Gyldensted C, Rosen BR. High resolution measurement of cerebral blood flow using intravascular tracer bolus passages. Part I: mathematical approach and statistical analysis. Magn Reson Med 1996;36:715–725.
2. Østergaard L, Soronsen AG, Kwong KK, Weisskoff RM, Gyldensted C, Rosen BR. High resolution measurement of cerebral blood flow using intravascular tracer bolus passages. Part II: experimental comparison and preliminary results. Magn Reson Med 1996;36:726–736.
3. Wirestam R, Andersson L, Østergaard L, Bolling M, Aunola J-P, Lindgren A, Geijer B, Holtås S, Stålberg F. Assessment of regional cerebral blood flow by dynamic susceptibility contrast MRI using different deconvolution techniques. Magn Reson Med 2000;43:691–700.
4. Østergaard L, Smith DF, Vestergaard-Pulsen P, Hansen SB, Gee AD, Gjedde A, Gyldensted C. Absolute cerebral blood flow and blood volume measured by magnetic resonance imaging bolus tracking: comparison with positron emission tomography values. J Cereb Blood Flow Metab 1998;18:425–432.
5. Østergaard L, Johansen P, Høst-Poulsen P, Vestergaard-Pulsen P, Asboe H, Gee AD, Hansen SB, Cold GE, Gjedde A, Gyldensted C. Cerebral blood flow measurements by magnetic resonance imaging bolus tracking: comparison with [^{15}O]H$_2$O positron emission tomography in humans. J Cereb Blood Flow Metab 1998;18:935–940.
6. Simonsen CZ, Østergaard L, Smith DF, Vestergaard-Pulsen P, Gyldensted C. Comparison of gradient- and spin-echo imaging: CBF, CBV, and MTT measurements by bolus tracking. J Magn Reson Imaging 2000;12:411–416.
7. Lassen NA, Perl W. Tracer kinetic methods in medical physiology. New York: Raven Press; 1979.
8. Yablonskiy DA, Haacke EM. Theory of NMR signal behavior in magnetically inhomogeneous tissue: the static dephasing regime. Magn Reson Med 1994;32:749–763.
9. Kiselev VG, Posse S. Analytical theory of susceptibility induced NMR signal dephasing in a cerebrovascular network. Phys Rev Lett 1998;81:5696–5699.
10. Kiselev VG, Posse S. Analytical model of susceptibility-induced MR signal dephasing: effect of diffusion in a microvascular network. Magn Reson Med 1999;41:499–509.
11. Meiboom S, Gill D. Modified spin echo method for measuring nuclear relaxation times. Rev Sci Instrum 1958;29:688–691.
12. Spees WM, Yablonskiy DA, Oswood MC, Ackerman JH. Water proton MR properties of human blood at 1.5 Tesla: magnetic susceptibility, T_1, T_2, T_2^*, and non-Lorenzian signal behavior. Magn Reson Med 2001;45:533–542.
13. Boxerman JL, Hamberg LM, Rosen BR, Weisskoff RM. MR contrast due to intravascular magnetic susceptibility perturbations. Magn Reson Med 1995;34:555–566.
14. Le Bihan D, Turner R, Patronas N. Diffusion MR imaging in normal brain and in brain tumor. In: Le Bihan D, editor. Diffusion and perfusion. Magnetic resonance imaging: applications to functional MRI. New York: Raven Press; 1995. p 134–140.
15. Schlenska G. Messungen der Oberflächen und der Volumenanteile des Gehirnes menschlicher Erwachsener mit neuen Methoden. Z Anat Entw Gesch 1969;128:47–59.
16. Pawlik G, Rackl A, Bing RJ. Quantitative capillary topography and blood flow in the cerebral cortex of cats: an in vivo microscopic study. Brain Res 1981;208:35–58.
17. Turner R. BOLD localization: the implications of vascular architecture. In: Proceedings of the 9th Annual Meeting of ISMRM, Glasgow, Scotland, 2001. p 288.
18. Friberg L. Methods for manipulation of regional brain perfusion, intracranal artery diameter and cerebral blood volume. In: Schmiedek P, Einhaupl K, Kirsch CM, editors. Stimulated cerebral blood flow: experimental findings and clinical significance. Berlin: Springer; 1991. p 141–149.
19. Büll U. Nuklearmedizin. Stuttgart, New York: Thieme; 1996.
20. Troprès I, Grimault S, Vaeth A, Glillon E, Julien S, Payen J-F, Lamalle L, Décorp M. Vessel size imaging. Magn Reson Med 2001;45:397–408.
21. Dennie J, Mandeville JB, Boxerman JL, Packard SD, Rosen BR, Weisskoff RM. NMR imaging of changes in vascular morphology due to tumor angiogenesis. Magn Reson Med 1998;40:793–799.
22. Hoogenraad F, Pouwels P, Hofman M, Reichenbach J, Sprenger M, Haacke E. Quantitative differentiation between BOLD models in fMRI. Magn Reson Med 2001;45:233–246.
23. Thulborn KR, Waterton JC, Matthews P, Radda GK. Oxygenation dependence of the transverse relaxation time of water protons in whole blood at high fields. Biochim Biophys Acta 1982;714:265–270.
24. Brooks RA, Vymazal J, Bulte JWM, Baumgarner CD, Tran V. Comparison of T2 relaxation in blood, brain, and ferritin. J Magn Res Imaging 1995;4:446–450.
25. Goldman M. Quantum description of high-resolution NMR in liquids. New York: Oxford University Press; 1988. p 226–262.
26. van Osch MPJ, Bakker CJG, Viergever MA. In vitro determination of MR-properties of gadolinium in flowing blood for arterial input function measurements. In: Proceedings of the 8th Annual Meeting of ISMRM, Denver, 2000. p 742.
27. Akbudak E, Hgu RM, Li Y, Conturo TE. ΔR^* and $\Delta\phi$ contrast agent perfusion effect in blood: quantitation and linear assessment. In: Proceedings of the 6th Annual Meeting of ISMRM, Sydney, Australia, 1998. p 1197.
28. Albert MS, Huang W, Lee J-H, Patlak CS, Springer CS. Susceptibility changes following bolus injections. Magn Reson Med 1993;29:700–708.
29. Landis CS, Li X, Telang FW, Coderre JA, Micca PL, Rooney WD, Latour LL, Vetek G, Palyka I, Springer Jr CS. Determination of the MRI contrast agent concentration time course in vivo following bolus injection: effect of equilibrium transcytolemmal water exchange. Magn Reson Med 2000;44:563–574.